

RSC Advances



This is an *Accepted Manuscript*, which has been through the Royal Society of Chemistry peer review process and has been accepted for publication.

Accepted Manuscripts are published online shortly after acceptance, before technical editing, formatting and proof reading. Using this free service, authors can make their results available to the community, in citable form, before we publish the edited article. This *Accepted Manuscript* will be replaced by the edited, formatted and paginated article as soon as this is available.

You can find more information about *Accepted Manuscripts* in the [Information for Authors](#).

Please note that technical editing may introduce minor changes to the text and/or graphics, which may alter content. The journal's standard [Terms & Conditions](#) and the [Ethical guidelines](#) still apply. In no event shall the Royal Society of Chemistry be held responsible for any errors or omissions in this *Accepted Manuscript* or any consequences arising from the use of any information it contains.

Linear and nonlinear optical properties for AA and AB stacking of Carbon Nitride polymorph (C₃N₄)

A. H. Reshak^{1,2}, Saleem Ayaz Khan^{1*}, S. Auluck³

¹*New Technologies - Research Center, University of West Bohemia, Univerzitni 8,
306 14 Pilsen, Czech republic*

²*Center of Excellence Geopolymer and Green Technology, School of Material Engineering,
University Malaysia Perlis, 01007 Kangar, Perlis, Malaysia*

³*Council of Scientific and Industrial Research - National Physical Laboratory Dr. K S
Krishnan Marg, New Delhi 110012, India*

Abstract

The linear and nonlinear optical susceptibilities of AA and AB stacking of carbon nitride polymorph were calculated using the all electron full potential linear augmented plane wave method based on density functional theory. The complex part of the dielectric function is calculated using the recent modified Becke and Johnson (mBJ) approximation which gives a better optical gap in comparison to Ceperley-Alder (CA) local density approximation, Perdew-Burke-Ernzerhof generalized gradient approximation, and the Engle-Vasko generalized gradient approximation. The complex dielectric function and other optical constants like refractive index, absorption coefficient, reflectivity and energy loss function are calculated and discussed in details. The calculated uniaxial anisotropy (-1.06 and -1.04) gives maximum value of birefringence (-0.89 and -0.87) which increases the suitability of both AA and AB stacking for a large second harmonic generation. The calculated second order susceptibility tensor components $|\chi_{333}^{(2)}(\omega)|$ at static limit are 19.4 pm/V and 59.6 pm/V for AA and AB stacking which increases to 34.2 pm/V and 106.7 pm/V at $\lambda = 1064$ nm. The first hyperpolarizability $\beta_{333}(\omega)$ for AA and AB stacking C₃N₄ for the dominant component $|\chi_{333}^{(2)}(\omega)|$ at static limit are calculated to be ($1.6 \times 10^{-30} esu$ and $9.6 \times 10^{-30} esu$) respectively.

Keywords: Carbon Nitride; Birefringence; Nonlinear optical susceptibilities;

*Corresponding author: *A.H.Reshak*

Tel. +420 777 729 583, E-mail address: maalidph@yahoo.co.uk

1. Introduction

Carbon nitride polymorph (C_3N_4), which comprises covalent bonds, has recently received much interest as a promising material in various applications. For instance as a photocatalyst, fuel cell electrode, light emitting apparatus and chemical sensor. In the past, Liu and Cohen¹ predict that β - C_3N_4 has compressibility comparable to that of diamond. The search for the distinct structure of C_3N_4 has a long history. Teter and Hemley² studied five types of C_3N_4 , including α - C_3N_4 , β - C_3N_4 , cubic- C_3N_4 , pseudocubic- C_3N_4 and graphitic C_3N_4 . Their computed results forecast that α - C_3N_4 and graphitic allotropes are energetically highly favored compared to β - C_3N_4 . Since then, much effort has been made for the synthesis of C_3N_4 . All sorts of methods have been utilized. These include vapor deposition, laser ablation and high pressure high-temperature procedures.³⁻⁵ Due to the chemical inertness of C_3N_4 , organizing dense C_3N_4 phases with large crystalline dimensions for explicit characterization is intricate. The g- C_3N_4 preparation has been described.⁶⁻¹⁹ A hypothetical material, C_3N_4 may have rather smaller bulk modulus than that of diamond as proposed by first-principles calculations^{20, 21}. These outcomes have inspired theoretical calculations²²⁻²⁶ and experimental efforts to synthesize and distinguish this compound²⁷⁻³⁸. From the synthesis of amorphous C-N films^{30, 32, 36}, small crystallites have been discovered in some of these films^{31, 33-35}. C_3N_4 is a chemically stable compound having a good thermal hardness and astonishing optical characteristics that make it suitable as a photocatalyst under visible light. The pursuit of C_3N_4 has potential for introducing new materials with band gap in the 2.6-3.0 eV range for energy, solar, and LED materials. However, it is important to note the recent advances in the fields of InGaN and AlInN alloy have been widely implemented in solar cells^{39, 40}, thermoelectricity^{41, 42}, and LEDs.⁴³⁻⁴⁷

Wang et al.⁴⁸ showed that in comparison with other oxides, g- C_3N_4 (having band gap of 2.7 eV) is metal free photocatalyst which can absorb more visible light and produce hydrogen from water. Tahir et al.⁴⁹ synthesized the tubular g- C_3N_4 and investigated the electrochemical properties which suggest it to be a good contestant for a supercapacitor and photocatalyst used for cleaning environment and energy storage purpose. Recently Wang et al.⁵⁰ synthesized the nanotube g- C_3N_4 material and demonstrated the intense fluorescence with a photoluminescent, reflecting the

applications as a blue light fluorescence material. This material also demonstrates the fabulous visible-light photocatalytic activity, suggesting the high usefulness of g-C₃N₄ nanotubes for gas storage, photocatalysis and light-emitting devices.⁵⁰

From above we notice that there is dearth of theoretical calculations for these materials. There exists a theoretical work based on the pseudopotential method which deals with only with valence electrons. Moreover the LDA-CP and GGA-PBE are also not much promising due to their band gap underestimation. It is well-known that the linear and nonlinear optical properties are very sensitive the band gap. Thus calculating the linear and nonlinear optical susceptibilities demands a very accurate energy gap value which should be very close to the experimental value. In our previous work⁵¹ we have calculated the electronic band structure, effective mass and valence electron charge density of AA and AB stacking of C₃N₄. Therefore as a natural extension we think it would be interesting to calculate the linear and nonlinear optical properties of AA and AB stacking of C₃N₄ using an all electron full potential linear augmented plane wave (FPLAPW) method which has proven to be the most precise technique within DFT to calculate the electronic structure of solids.^{52, 53} In order to explore the effect of different exchange correlation potentials we have performed calculations for four type of exchange and correlation potentials. Thus, based on our previous experiences with this approach, we expect to get more accurate results as compared to the pseudopotential method.

2. Crystal structure and computational details

The crystal structure of AA and AB stacking of C₃N₄ polymorphs is stable in hexagonal symmetry having space group P-6m2. The crystallographic data of C₃N₄ polymorphs are taken from David et al.⁵⁴. The crystal structure of AA and AB stacking are shown in Fig.1(a, b). We have employed the full potential linear augmented plane wave (FPLAPW) within Wien2k package⁵⁵. Four schemes namely Ceperley-Alder (CA) local density approximation (LDA-CA)⁵⁶, Perdew-Burke-Ernzerhof generalized gradient approximation (PBE-GGA)⁵⁷, Engel-Vosko generalized gradient approximation (EV-GGA)⁵⁸ and a recent modified Becke and Johnson (mBJ) scheme⁵⁹ were used for the self-consistent calculations. The convergence parameters ($R_{MT}K_{max}$) that used to control size of the basis set for present calculation is set to be 7.0. The expression R_{MT} represent

muffin-tin (MT) sphere radius and K_{\max} symbolize the magnitude of largest K vector in plane wave expansion. The selected muffin-tin (MT) sphere radii for C and N is 1.24 atomic units (a.u.) in both AA and AB stacking of C_3N_4 polymorphs. The wave function inside the MT sphere was expanded up to $l_{\max} = 10$ where as the Fourier expansion of the charge density was expanded up to $G_{\max} = 12$ (a.u.)⁻¹. The cutoff energy was selected as 6.0 Ryd. The convergence of self consistent calculations was done when the difference in total energy of the crystal did not exceed 10^{-5} Ryd for succeeding steps. The self consistent calculations were obtained for both cases by 308 **k** points in irreducible Brillouin zone (IBZ).

3. Result and discussions

3.1. Linear Optical Properties

The complex dielectric function $\varepsilon(\omega)$ of the material is linked to the energy band structure. The overall band behavior of a solid can be explained by optical spectroscopy analysis of $\varepsilon(\omega)$ ⁶⁰. The complex dielectric function $\varepsilon(\omega) = \varepsilon_1(\omega) + i\varepsilon_2(\omega)$ is the keynote factor for calculating the optical properties of the materials. The dispersion of dielectric function contains intra- and inter-band transitions. The intra-band transitions are present only in metals. In semiconductors only the inter-band transitions are present. Further the inter-band transitions are divided into direct and indirect band transitions. The contribution of the phonons associated from lattice vibration in indirect inter-band transition are ignored because of small the contribution and only direct band to band transition of electron are taken into account. The correct energy eigenvalues and electron wave functions are necessary to calculate the dispersion of dielectric function $\varepsilon(\omega)$. These are natural output of the band structure calculation. The crystal structure symmetry (hexagonal) of AA and AB stacking of C_3N_4 contains two non-zero principal diagonal dielectric tensor components $\varepsilon^{xx}(\omega) = \varepsilon^{yy}(\omega)$ and $\varepsilon^{zz}(\omega)$ along **a**, **b** and **c** crystallographic axis. These are required to complete the explanation of the linear optical properties. These components can be calculated using the expression taken from Ref. 61;

$$\varepsilon_2^{ij} = \frac{4\pi^2 e^2}{Vm^2 \omega^2} \times \sum_{mn'\sigma} \langle kn\sigma | p_i | kn'\sigma \rangle \langle kn'\sigma | p_j | kn\sigma \rangle \times f_{kn} (1 - f_{kn'}) \delta(E_{kn'} - E_{kn} - \hbar\omega) \quad (1)$$

where m and e represent mass and charge of electron, respectively and ω stands for electromagnetic radiation interacting with the crystal, V stands for unit cell volume, The p notation in bracket represent the momentum operator, $|kn\sigma\rangle$ stand for the crystal wave function with crystal momentum k , and σ spin symbolize the eigenvalue E_{kn} . The Fermi distribution function (f_{kn}) makes sure the counting of transition from occupied to unoccupied state and $\delta(E_{kn'} - E_{kn} - \hbar\omega)$ shows the condition for conservation of total energy.

The structures in the optical response are caused by the electric-dipole transitions between the valence and the conduction bands. In order to identify these structures we need to look at the magnitude of the optical matrix elements. The observed structures would correspond to those transitions that have large optical matrix elements. The calculated absorptive and dispersive part of AA and AB stacking of C_3N_4 by LDA, GGA-PBE, EVGGA and mBJ, are shown in Fig.2(a, b, c, d). This elucidates that mBJ approach shows a better optical gap compared to LDA, GGA and EVGGA. According to our previous experience with mBJ⁶²⁻⁶⁷ we find that mBJ brings the energy gap closer to the experimental one therefore we preferred mBJ scheme for calculations of the linear and nonlinear optical properties as they are very sensitive to the band gap. Fig.2 (e, f) shows the imaginary part of optical dielectric tensor components for AA and AB stacking of C_3N_4 . The calculated $\varepsilon_2(\omega)$ for AA stacking shows a high transparency optical gap up to 2.59 eV while for AB stacking the transparency region increases to 2.99 eV. The first peak in both cases represents transition of electron from valence band maximum to conduction band minimum. Similarly the rest of the peaks represents transitions of electrons from lower occupied bands to upper unoccupied bands. There is a considerable anisotropy between $\varepsilon_2^{xx}(\omega)$ and $\varepsilon_2^{zz}(\omega)$ for whole energy range of AA and AB stacking of C_3N_4 . The real part of the optical dielectric tensor components is linked to the electric polarizability of the material which can be calculated from imaginary part using Kramers-Kronig relation⁶⁸;

$$\varepsilon_1(\omega) = 1 + \frac{2}{\pi} P \int_0^{\infty} \frac{\omega' \varepsilon_2(\omega')}{\omega'^2 - \omega^2} d\omega' \quad (2)$$

Fig.2(g, h) represents the real part of dielectric tensor components for AA- and AB-stacking. The calculated uniaxial anisotropy $\delta\varepsilon = [(\varepsilon_0^{zz} - \varepsilon_0^{xx}) / \varepsilon_0^{\text{tot}}]$ presented in Table 1, indicates considerable anisotropy⁶⁹ between the spectral components of the dielectric function of AA and AB stacking. Table 1 also elucidates the other optical parameters of AA and AB stacking of C₃N₄ in comparison with diamond, β -C₃N₄, α -C₃N₄, γ -C₃N₄ and pc-C₃N₄. Fig.2(i, j) shows the calculated refractive index $n(\omega)$ of AA and AB stacking. The refractive index is also related to the electric polarizability of the material. The static value of refractive index for two non-zero tensor components of AA and AB stacking are directly linked to $n(0)$ by the relation $n(\omega) = \sqrt{\varepsilon_1(0)}$, as shown in Table 1. The most responsible component which increases the refractive index of C₃N₄ is $n^{xx}(\omega)$ while $n^{zz}(\omega)$ shows a negligible role in both stacking cases. When the energy of electromagnetic (EM) waves is increased the $n^{xx}(\omega)$ also increases and achieves a maximum value at 4.9 and 4.8 eV for AA and AB stacking, respectively. Further increasing the energy cause sharp decrease in $n^{xx}(\omega)$. The $n^{xx}(\omega)$ curve crosses the unity at 5.5 eV. This shows the high luminescent nature of AA stacking as compared AB stacking.

The absorption coefficient of the two dielectric tensor components shows a considerable anisotropy between the two components $I^{xx}(\omega)$ and $I^{zz}(\omega)$ for both AA and AB stacking. For both, $I^{xx}(\omega)$ shows dominancy while $I^{zz}(\omega)$ exhibits a minor role. In AA stacking of C₃N₄, the first peak of $I^{xx}(\omega)$ shows maximum absorption of about $175 \times 10^4 \text{ cm}^{-1}$ around 5.4 eV, while in AB-stacking the first peak of $I^{xx}(\omega)$ shifts to 5.2 eV with a smaller value of absorption coefficient ($167 \times 10^4 \text{ cm}^{-1}$) as shown in Fig.2(k, l). The two components of the reflectivity $R^{xx}(\omega)$ and $R^{zz}(\omega)$ also shows considerable anisotropy. $R^{xx}(\omega)$ plays a leading role with maximum reflection of 62 % (AA stacking) and 56 % (AB stacking) around 5.5 eV whereas $R^{zz}(\omega)$ shows a negligible role except in the higher energy range (13.5 eV) as shown in Fig.2(m, n).

The energy loss spectrum is related to the energy loss of a fast moving electron in the crystal. Fig.2(o, p) elucidates considerable anisotropy between $L^{xx}(\omega)$ and $L^{zz}(\omega)$ in AA and AB stacking of C_3N_4 . In the energy range between 2.59 eV and 5.0 eV for AA stacking and from 2.99 eV to 4.60 eV in AB stacking, $L^{zz}(\omega)$ is the dominant component. As one moves to higher energy range $L^{xx}(\omega)$ becomes dominant in both stacking by showing maximum value of energy loss spectrum around 9.5 eV.

The calculated birefringence $\Delta n(\omega)$ of AA and AB stacking of C_3N_4 polymorph are shown in Fig.2(q, r). Birefringence is given by the relation $\Delta n = n_e - n_o$. Where n_e and n_o are the refractive indices categorized in extraordinary and ordinary ray of polarized light. $\Delta n(\omega)$ is very important in the non-absorbing region below the gap⁷⁰. The calculated static values of $\Delta n(\omega)$ are shown Table 1.

3.2. Nonlinear Optical Properties

The present compounds have only one independent dominant tensor components $\chi_{333}^{(2)}(-2\omega; \omega; \omega)$. The number in the subscript represents the three polarization directions along x, y and z direction. The first order response only deals with inter-band transitions and involves the square matrix elements giving positive values for $\varepsilon_2(\omega)$. The second harmonic generation (SHG) involves 2ω resonance in accumulation with 1ω resonance which are furthermore separated into inter-band $\chi_{inter}^{(2)}(-2\omega; \omega; \omega)$, intra-band $\chi_{intra}^{(2)}(-2\omega; \omega; \omega)$ term along with modulation of intra-band on inter-band term $\chi_{mod}^{(2)}(-2\omega; \omega; \omega)$. The expressions of the complex second-order nonlinear optical susceptibility tensor are given in the Refs. 71-75.

Since the nonlinear optical properties are very sensitive to the band gap of the material as compared to linear optical properties therefore, we have selected to show the results obtained by mBJ scheme because it produces better band splitting and hence gives a band gap value close to the experimental one. The importance of the static values of dielectric tensor components of optical susceptibilities cannot be ignored because it is used to calculate the relative frequency of SHG efficiency⁷⁵. The real and imaginary part of second

order optical susceptibilities $\chi_{333}^{(2)}$ of both AA and AB stacking of C_3N_4 are shown in Fig.3(a, b). The maximum peak value of $\text{Re } \chi_{333}^{(2)}$ and $\text{Im } \chi_{333}^{(2)}$ for AA stacking are 300 pm/V and 110 pm/V which are located at 3.1 eV and 3.5 eV. In AB stacking both peaks shift to 2.8 eV and 3.25 eV with increasing the peak heights to be 610 pm/V and 215 pm/V for both $\text{Re } \chi_{333}^{(2)}$ and $\text{Im } \chi_{333}^{(2)}$.

Fig.3(c, d) shows the intra- and inter- band contribution of ω and 2ω resonance for AA and AB stacking of C_3N_4 , respectively. One can see that ω resonance is smaller than 2ω resonance in both cases. The maximum peaks of inter- and intra- band of 2ω resonance in AA stacking are located at 2.9 eV which illuminates value of $13 \times 10^{-7} \text{esu}$ and $-22.5 \times 10^{-7} \text{esu}$. For AB stacking these peaks are situated at 2.7 eV with maximum value of $27.5 \times 10^{-7} \text{esu}$ and $-49.0 \times 10^{-7} \text{esu}$ for inter- and intra- band contribution of 2ω respectively. Similarly when one moves from AA stacking to AB stacking, both contributions (inter- and intra-) of 1ω resonance shifts to lower energy with increasing value of $\text{Im } \chi_{333}^{(2)}$. It is also clear that $\text{Im } \chi_{333}^{(2)}$ shows a zero value below half the band gap ($E_g/2$). The 2ω resonance starts to contribute at energy $> E_g/2$, while ω resonance begins to contribute at energies above E_g . The clear vision of the ω and 2ω resonance can be seen in Fig.3(e, f). The upper panel of Fig.3(e, f) show the calculated value of $|\chi_{333}^{(2)}(\omega)|$ for the dominant tensor component. The value of $|\chi_{333}^{(2)}(\omega)|$ at the static limit $|\chi_{333}^{(2)}(0)|$ is 19.4 pm/V for AA stacking and 59.6 pm/V for AB stacking. At $\lambda = 1064 \text{ nm}$ the $|\chi_{333}^{(2)}(\omega)|$ value increased to be 34.2 pm/V for AA stacking and 106.7 pm/V for AB stacking.

To analyze the features of the calculated absolute value of the dominant component $|\chi_{333}^{(2)}(\omega)|$ it would be worthwhile helpful to compare $|\chi_{333}^{(2)}(\omega)|$ (Fig.3e,f –upper panel) with the absorptive part of the corresponding dielectric function $\varepsilon_2(\omega)$ as a function of both $\omega/2$ and ω (Fig.3e,f -lower panel). The 2ω resonance is responsible for spectral structure formation in the energy range from 1.29 eV to 2.59 eV (1.50 eV to 2.99 eV) for AA stacking (AB stacking). The subsequent structure ranges from 2.59 eV to 6.80 eV (2.99 eV to 6.80 eV) for AA stacking (AB stacking) is fashioned by the combined effect of ω and 2ω resonance and the rest of the structure is formed by only ω resonance. The calculated

values of second order susceptibility for AA and AB stacking of C_3N_4 are listed in Table 2 in comparison to the experimental and theoretical results of ZnS, GaN and GaAs.

We also have calculated the first hyperpolarizability β_{ijk} vector component along dipole moment direction using the static value of $|\chi_{333}^{(2)}(\omega)|$ and the calculated density for AA stacking and AB stacking (Table 1), using the expression given in ref. 76. The calculated values of $\beta_{333}(\omega)$ are $1.6 \times 10^{-30} esu$ and $9.6 \times 10^{-30} esu$ for AA and AB stacking of C_3N_4 , respectively.

4. Conclusions

We have calculated the linear and nonlinear optical properties of AA and AB stacking of carbon nitride polymorph using all electron full potential linear augmented plane wave method based on DFT within the frame work of Wien2k code. The exchange correlation energy was solved using four schemes namely Ceperley-Alder (CA) local density approximation, Perdew-Burke-Ernzerhof generalized gradient approximation, Engel-Vosko generalized gradient approximation and recent modified Becke and Johnson (mBJ) approximation. We have calculated and discussed in detail the complex dielectric function and the other optical constants such as refractive index, absorption coefficient, reflectivity and energy loss function. The uniaxial anisotropy ($\delta\varepsilon$) was calculated to be -1.06 for AA stacking and -1.04 AB stacking which ensures higher value of birefringence. The value of birefringence at the static limit $\Delta n(0)$ is -0.89 for AA stacking and -0.87 for AB stacking. The values of $\delta\varepsilon$ and $\Delta n(0)$ predict that both AA and AB stacking posses large second harmonic generation. The second order susceptibility tensor components $|\chi_{333}^{(2)}(\omega)|$ for AA-stacking (AB- stacking) were calculated at static limit and at $\lambda= 1064$ nm, these are 19.4 pm/V and 34.2 pm/V (59.6 pm/V and 106.7 pm/V). In additional we have calculated the first hyperpolarizability $\beta_{333}(\omega)$ using the static value of $|\chi_{333}^{(2)}(\omega)|$. These are $1.6 \times 10^{-30} esu$ and $9.6 \times 10^{-30} esu$ for AA and AB stacking of C_3N_4 , respectively.

Acknowledgments

The result was developed within the CENTEM project, reg. no. CZ.1.05/2.1.00/03.0088, co-funded by the ERDF as part of the Ministry of Education, Youth and Sports OP RDI programme. SA would like to thank CSIR-NPL for financial assistance.

Reference

- [1] A. Y. Liu, M. L. Cohen, *Science*, 1989, **245**, 841-2.
- [2] David M. Teter, Russell J. Hemley, *Science*, 1996, **271**, 53-55.
- [3] D. W. He, F. X. Zhang, X. Y. Zhang, Z. C. Qin, M. Zhang, R. P. Liu et al. *J Mater Res.*, 1998, **13**, 3458-62.
- [4] Z. Zhang, H. Guo, G. Zhong, F. Yu, Q. Xiong, X. Fan, *Thin Solid Films*, 1999, **346**, 96-9.
- [5] Y. Peng, T. Ishigaki, S. Horiuchi, *Appl Phys Lett.*, 1998, **73**, 3671-3.
- [6] V. N. KhAB shesku, J. L. Zimmerman, J. L. Margrave, *Chem Mater*, 2000, **12**, 3264-70.
- [7] M. J. Bojdys, J. O. Muller, M. Antonietti, A. Thomas, *Chem-Eur J*, 2008, **14**, 8177-82.
- [8] A. Thomas, A. Fischer, F. Goettmann, M. Antonietti, J. O. Muller, R. Schlogl et al., *J Mater Chem.*, 2008, **18**, 4893-908.
- [9] X. Li, J. Zhang, L. Shen, Y. Ma, W. Lei, Q. Cui et al. *Appl Phys A-Mater*, 2009, **94**, 387-92.
- [10] D. R. Miller, J. R. Holst, E. G. Gillan, *Inorg Chem.*, 2007, **46**, 2767-74.
- [11] H. Montigaud, B. Tanguy, G. Demazeau, I. Alves, S. Courjault, *J Mater Sci.*, 2000, **35**, 2547-52.
- [12] S. M. Lyth, Y. NABe, S. Moriya, S. Kuroki, M. A. Kakimoto, J. I. Ozaki, et al. *J Phys Chem C*, 2009, **113**, 20148-51.
- [13] C. Li, X. G. Yang, B. J. Yang, Y. Yan, Y. T. Qian, *Mater Chem Phys.*, 2007, **103**, 427-32.
- [14] K. Gibson, J. Glaser, E. Milke, M. Marzini, S. Tragl, M. Binnewies et al., *Mater Chem Phys.*, 2008, **112**, 52-6.

- [15] J. L. Zimmerman, R. Williams, V. N. KhABshesku, J. L. Margrave, *Nano Lett.*, 2001, **1**, 731-4.
- [16] H. A. Ma, X. P. Jia, L. X. Chen, P. W. Zhu, W. L. Guo, X. B. Guo, et al., *J Phys Condens Mat.*, 2002, **14**, 11269.
- [17] G. Goglio, D. Andrault, S. Courjault, G. Demazeau. *High Press Res.*, 2002, **22**, 535-7.
- [18] J. Kouvetakis, M. Todd, B. Wilkens, A. Bandari, N. Cave. *Chem Mater*, 1994, **6**, 811-4.
- [19] E. G. Gillan, *Chem Mater*, 2000, **12**, 3906-12.
- [20] A. Y. Liu and M. L. Cohen, *Science*, 1989, **245**, 841.
- [21] A. Y. Liu and M. L. Cohen, *Phys. Rev. B*, 1990, **41**, 10727.
- [22] J. L. Corkill and M. L. Cohen, *Phys. Rev. B: Condens. Matter Mater. Phys.*, 1993, **48**, 17622.
- [23] H. Yao and W. Y. Ching, *Phys. Rev. B: Condens. Matter Mater. Phys.*, 1994, **50**, 11231.
- [24] J. Ortega and O. F. Sankey, *Phys. Rev. B: Condens. Matter Mater. Phys.*, 1995, **51**, 2624.
- [25] Y. Guo and W. A. Goddard, *Chem. Phys. Lett.*, 1995, **237**, 72.
- [26] J. Hu, *Applied physics Lett.*, 1995, **89**, 261117.
- [27] T. Sekine, H. Kanda, Y. Bando, M. Yokohama, K. Hojou, *J. Mat. Sci. Lett.*, 1990, **9**, 1376.
- [28] L. Maya, D. R. Cole, E. W. Hagaman, *J. Am. Ceram. Soc.*, 1991, **74**, 1686.
- [29] J. J. Cuomo, P. A. Leary, D. Yu, W. Reuter, M. Frisch, *J. Vac. Sci. Technol.*, 1976, **16**, 299.
- [30] H. X. Han and B. J. Feldman, *Solid State Commun.*, 1988, **65**, 921.
- [31] C. Niu, Y. Z. Liu, C. M. Lieber, *Science*, 1993, **261**, 334.
- [32] D. Marton, K. J. Boyd, A. H. Al-Bayati, S. S. Todorov, J. W. RABlais, *Phys. Rev. Lett.*, 1994, **73**, 118.
- [33] K. M. Yu, M. L. Cohen, E. E. Haller, W. L. Hansen, A. Y. Lu, I. C. Wu, *Phys. Rev.*, 1994, B **49**, 5034.

- [34] J. P. Riviere, D. Texier, J. Delafond, M. Jaouen, E. L. Mathe, J. Chaumont, *Mater. Lett.*, 1995, **22**, 115.
- [35] Z. M. Ren et al., *Phys. Rev. B*, 1995, **51**, 5274.
- [36] Y. Yang, K. A. Nelson, F. Adibi, *J. Mater. Res.*, 1995, **10**, 41.
- [37] M. H. V. Huynh, M. A. Hiskey, J. G. Archuleta and E. L. Roemer, *Angew. Chem., Int. Ed.*, 2004, **43**, 5658; 2005, **44**, 737.
- [38] H. R. Phillip and E. A. Taft, *Phys. Rev.*, 1964, **136**, A1445.
- [39] E. C. Young, F. Wu, A. E. Romanov, D. A. Haeger, S. Nakamura, S. P. Denbaars, D. A. Cohen and J. S. Speck, *Appl. Phys. Lett.*, 2012, **101**, 5.
- [40] C. J. Neufeld, N. G. Toledo1, S. C. Cruz, M. Iza, S. P. DenBaars and U. K. Mishra *Appl. Phys. Lett.*, 2008, **93**, 143502.
- [41] J. Zhang, H. Tong, G. Liu, J. A. Herbsommer, G. S. Huang and N. Tansu, *J. Appl. Phys.*, 2011, **109**, 053706.
- [42] Jing Zhang, Songul Kutlu, Guangyu Liu and Nelson Tansu, *J. Appl. Phys.*, 2011, **110**, 043710.
- [43] D. Feezell, et al, *J. Display Technology*, 2013, **9**, 190-198.
- [44] H. Zhao, G. Liu, J. Zhang, J. D. Poplawsky, V. Dierolf, and N. Tansu, *Optics Express*, 2011, **19**, A991-A1007.
- [45] R. A. Arif, H. Zhao and N. Tansu, *Appl. Phys. Lett.*, 2008, **92**, 011104.
- [46] H. Zhao1, R. A. Arif and N. Tansu, *J. Appl. Phys.*, 2008, **104**, 043104.
- [47] K. T. Delaney, P. Rinke and C. G. Van de Walle, *Appl. Phys. Lett.*, 2009, **94**, 191109.
- [48] X. C. Wang, K. Maeda, A. Thomas, K. Takanabe, G. Xin, J. M. Carlsson, K. Domen, M. Antonietti, *Nat. Mater.*, 2009, **8**, 76.
- [49] M. Tahir, C. Cao, F. K. Butt, F. Idrees, N. Mahmood, I. Aslam, Z. Ali, M. Tanvir, M. Rizwan and T. Mahmood, *J. Mater. Chem. A*, 2013, **1**, 13949.
- [50] S. Wang, C. Li, T. Wang, P. Zhang, A. Li and J. Gong, *J. Mater. Chem. A*, 2014, **2**, 2885
- [51] A. H. Reshak, S. A. Khan and S. Auluck, *RSC Adv.*, 2014, **4**, 6957–6964.
- [52] S. Gao, *Computer Physics Communications*, 2003, **153**, 190-198.
- [53] K. Schwarz, *Journal of Solid State Chemistry*, 2003, **176**, 319-328.

- [54] P. Balaha, K. Shewartz, G. K. H. Madsen, D. Kvsnicka, J. Luitz, WIEN2K, an Augmented plane wave +local orbitals program for calculating crystals properties, Karlheinz Schewartz, Techn. Universitat, Wien Austria, 2001, ISBN 3-9501031-1-2.
- [55] D. M. Ceperley and B. I. Alder, Phys. Rev. Lett., 1980, **45**, 566.
- [56] J. P. Perdew, K. Burke and M. Ernzerhof, Phys. Rev. Lett., 1996, **77**, 3865.
- [57] E. Engel and S. H. Vosko, Phys. Rev. B: Condens. Matter Mater. Phys., 1993, **47**, 13164.
- [58] F. Tran and P. Blaha, Phys. Rev. Lett., 2009, **102**, 226401.
- [59] S. A. Khan, A. H. Reshak, Int. J. Electrochem. Sci., 2013, **8**, 9459 – 9473
- [60] A. H. Reshak, S. A. Khan, Computational Material Science, 2013, **78**, 91-97.
- [61] A. Delin, P. Ravindran, O. Eriksson, J. M. Wills, Int. J. Quant. Chem., 1998, **69** 349-358.
- [62] A. H. Reshak, X. Chen, S. Auluck, H. Kamarudin, Materials Chemistry and Physics, 2012, **137**, 346-352.
- [63] A. H. Reshak, X. Chen, S. Auluck, and H. Kamarudin, Journal of Applied Physics, 2012, **112**, 053526.
- [64] A. H. Reshak, I. V. Kityk, O. V. Parasyuk, A. O. Fedorchuk, Z. A. Alahmed, N. AlZayed, H. Kamarudin, S. Auluck, J Mater Sci., 2013, **48**, 1342–1350.
- [65] A. H. Reshak, I. V. Kityk, O. V. Parasyuk, H. Kamarudin, S. Auluck, J. Phys. Chem. B, 2013, **117**, 2545–2553
- [66] M. Benkraouda, N. Amrane, J Alloys Compds, 2013, **546**, 151–156.
- [67] S. Guo, B. Liu, Journal of Magnetism and Magnetic Materials, 2012, **324**, 2410–2415
- [68] H. Tributsch, *Naturforsch*, 1977, **32A**, 972.
- [69] A. H. Reshak, X. Chen, S. Auluck, I. V. Kityk, J. Chem. Phys., 2008, **129**, 204111
- [70] A. H. Reshak, S. Auluck, and I. V. Kityk, Phys Rev. B, 2007, **75**, 245120.
- [71] S. Sharma, J. K. Dewhurst, C. Ambrosch-Draxl, Phys Rev B, 2003, **67**, 165332.
- [72] A. H. Reshak, Ph.D. thesis, Indian Institute of Technology-Roorkee, India, 2005.

- [73] A. H. Reshak, J Chem Phys., 2006, **125**, 014708.
- [74] A. H. Reshak, J Chem Phys., 2006, **124**, 014707.
- [75] A. H. Reshak, H. Kamarudin, S. Auluck, J. Mat. Sci., 2013, **48**, 1955-1965.
- [76] R. Y. Boyed, Principles of non linear optics. Academic Press is an imprint of Elsevier. ISBN: 978-0-12-369470-6.
- [77] J.W. Zou, K. Reichelt, K. Schmidt, B. Dischler, Journal of Applied Physics, 1989, **65**, 3914 – 3918.
- [78] J. Hu, P. Yang, and C. M. Lieber, Physical Review B. **57** (6), R3185
- [79] L. C. Ming, P. Zinin, Y. Meng, X. R. Liu, S. M. Hong, and Y. Xie, Journal of Applied Physics, 2006, **99**, 033520.
- [80] D. T. F. Marple, J. Appl. Phys., 1964, **35**, 539.
- [81] James L. P. Hughes, Y. Wang, and J. E. Sipe, Phys Rev. B, 1997, **55**(20), 13630.
- [82] B.F. Levine and C.G. Bethea, Appl. Phys. Lett., 1972, **20**, 272.

Table 1: Calculated linear and non linear optical constants of C₃N₄

	Graphitic-C ₃ N ₄ (AA Stacking)	Graphitic-C ₃ N ₄ (AB Stacking)	Diamond	β-C ₃ N ₄	α-C ₃ N ₄	γ-C ₃ N ₄	pc-C ₃ N ₄
Space group	$P\bar{6}2m$	$P\bar{6}2m$	$Fd\bar{3}m$	$P6_3/m$	$P3_1c$	$Fd\bar{3}m$	$P4\bar{2}m$
Volume (Å ³)	73.8 [*]	147.1 [*]	44.2 ^a	85.49 ^a	170.63 ^a	307.91 ^a	40.52 ^a
E_g (eV)	2.59 [*]	2.99 [*]	5.72 ^a , 5.47 ^b	3.825 ^a	4.672 ^a	1.445 ^a	2.843 ^a
$\epsilon_1^{xx}(0)$	3.86 [*]	3.85 [*]	5.70 ^b	4.533 ^a	4.288 ^a	6.275 ^a	5.190 ^a
$\epsilon_1^{zz}(0)$	1.15 [*]	1.18 [*]	5.79 ^a	4.755 ^a	4.296 ^a		
$n^{xx}(0)$	1.95 [*]	1.96 [*]	2.417 ^c	2.129 ^a	2.071 ^a	2.505 ^a	2.278 ^a
$n^{zz}(0)$	1.06 [*]	1.09 [*]	2.417 ^c	2.181 ^a	2.072 ^a	2.505 ^a	
$\Delta n(0)$	-0.89 [*]	-0.87 [*]					
$\delta\epsilon$	-1.06 [*]	-1.04 [*]					
Density (g/cm ³)	2.0215 [*]	2.0201 [*]	3.51 ^d	3.57 ^e	3.585 ^f	2.620 ^{g*}	3.811 ^f

*Present work

^aTheoretical work Ref.[26]

^bExperimental work Ref.[37]

^cExperimental work Ref.[38]

^dExperimental work Ref.[77]

^eExperimental work Ref.[78]

^fTheoretical work Ref.[2]

^gExperimental work Ref.[79]

Table 2: Calculated nonlinear second order susceptibility and birefringence

	Graphitic-C ₃ N ₄ (AA Stacking)	Graphitic-C ₃ N ₄ (AB Stacking)	ZnS	GaN	GaAs
$ \chi_{333}^{(2)}(0) $	19.4 [*]	59.6 [*]	16.0 ^a	6.0 ^b	34.0 ^c
$ \chi_{333}^{(2)}(\omega) $	34.2 [*]	106.7 [*]			
at $\lambda = 1064nm$					

*This work

^aExperimental work Ref.[80]

^bTheoretical work Ref.[81]

^cExperimental work Ref.[82]

Figure Captions

Fig.1: Crystal structure of C₃N₄ (a) AA-stacking (b) AB-stacking

Fig.2: (a) Calculated $\varepsilon_2^{xy}(\omega)$ for AA-stacking C₃N₄; (b) Calculated $\varepsilon_2^{xy}(\omega)$ for AB-stacking C₃N₄; (c) Calculated $\varepsilon_1^{xy}(\omega)$ for AA-stacking C₃N₄; (d) Calculated $\varepsilon_1^{xy}(\omega)$ for AB-stacking C₃N₄; (e) Calculated $\varepsilon_2^{xx}(\omega)$ and $\varepsilon_2^{zz}(\omega)$ for AA-stacking; (f) Calculated $\varepsilon_2^{xx}(\omega)$ and $\varepsilon_2^{zz}(\omega)$ for AB-stacking; (g) Calculated $\varepsilon_1^{xx}(\omega)$ and $\varepsilon_1^{zz}(\omega)$ AA-stacking C₃N₄; (h) Calculated $\varepsilon_1^{xx}(\omega)$ and $\varepsilon_1^{zz}(\omega)$ AB-stacking C₃N₄; (i) Calculated $n^{xx}(\omega)$ and $n^{zz}(\omega)$ for AA-stacking; (j) Calculated $n^{xx}(\omega)$ and $n^{zz}(\omega)$ for AB-stacking; (k) Calculated $I^{xx}(\omega)$ and $I^{zz}(\omega)$ for AA-stacking; (l) Calculated $I^{xx}(\omega)$ and $I^{zz}(\omega)$ for AB-stacking; (m) Calculated $R^{xx}(\omega)$ and $R^{zz}(\omega)$ for AA-stacking; (n) Calculated $R^{xx}(\omega)$ and $R^{zz}(\omega)$ for AB-stacking; (o) Calculated $L^{xx}(\omega)$ and $L^{zz}(\omega)$ for AA-stacking; (p) Calculated $L^{xx}(\omega)$ and $L^{zz}(\omega)$ for AB-stacking; (q) Calculated birefringence (Δn) for AA-stacking; (r) Calculated birefringence (Δn) for AB-stacking;

Fig.3: (a) Calculated real and imaginary of $\chi_{333}^{(2)}(\omega)$ for AA-stacking; (b) Calculated real and imaginary of $\chi_{333}^{(2)}(\omega)$ for AB-stacking; (c) Calculated total $\text{Im} \chi_{333}^{(2)}(-2\omega; \omega; \omega)$ along

with inter ($2\omega/\omega$) and intra ($2\omega/\omega$) band contribution for AA-stacking; (d) Calculated total $\text{Im}\chi_{333}^{(2)}(-2\omega;\omega;\omega)$ along with inter ($2\omega/\omega$) and intra ($2\omega/\omega$) band contribution for AB-stacking; (e) Calculated $|\chi_{333}^{(2)}(\omega)|$ and $\epsilon_2^{\text{average}}(\omega)$ along with $\epsilon_2^{\text{average}}(\omega/2)$ for AA-stacking; (f) Calculated $|\chi_{333}^{(2)}(\omega)|$ and $\epsilon_2^{\text{average}}(\omega)$ along with $\epsilon_2^{\text{average}}(\omega/2)$ for AB-stacking

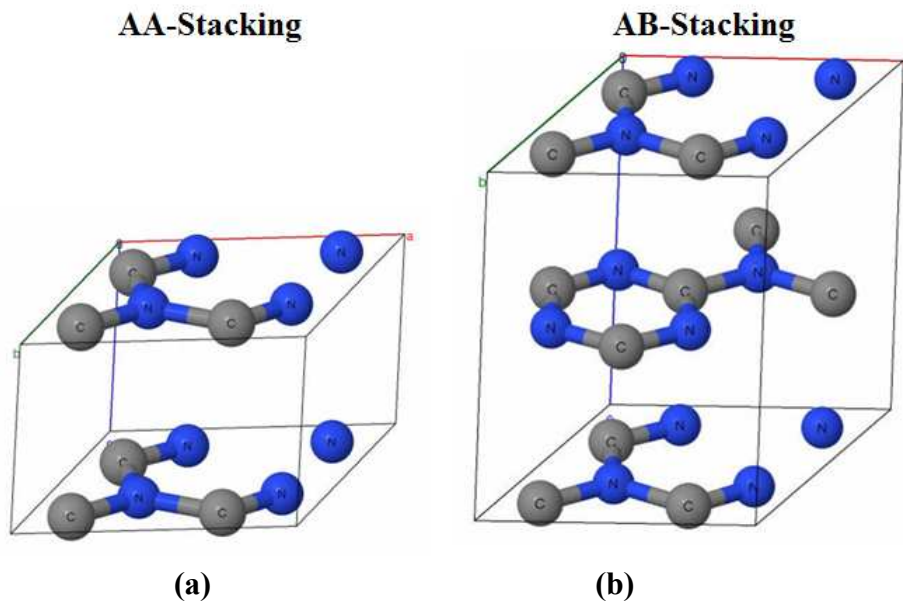
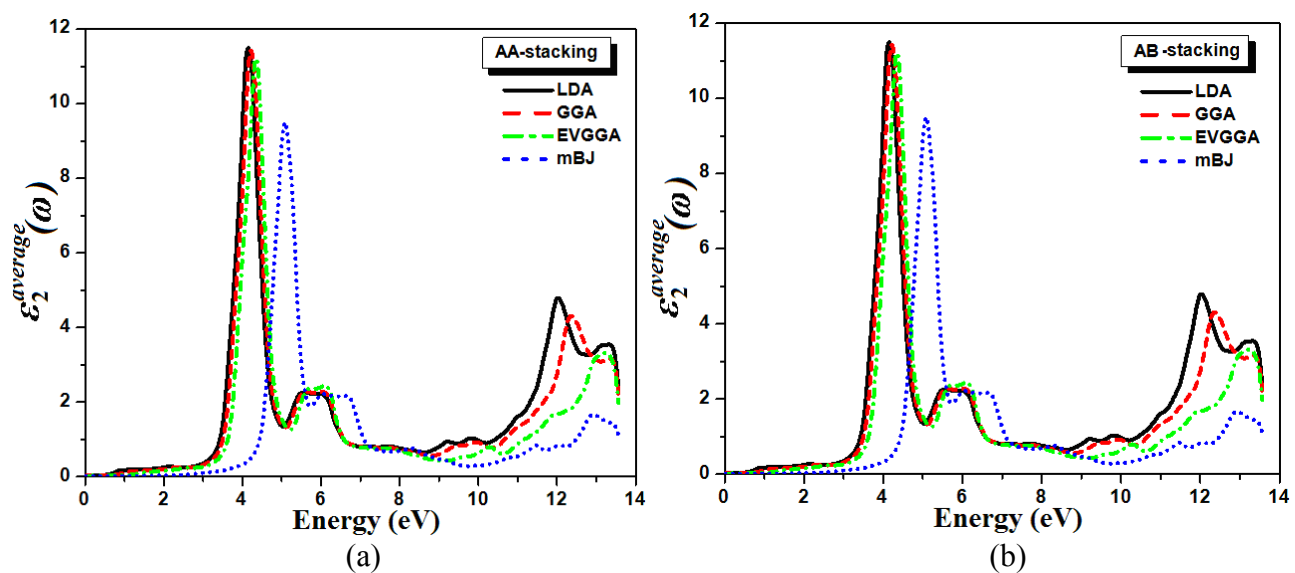
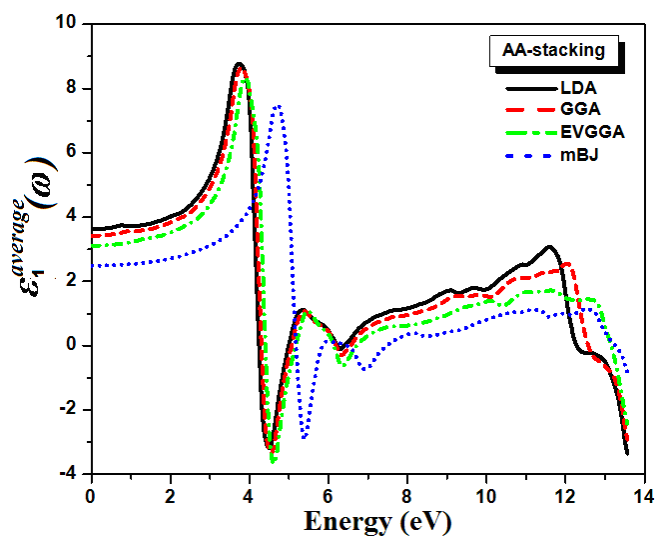
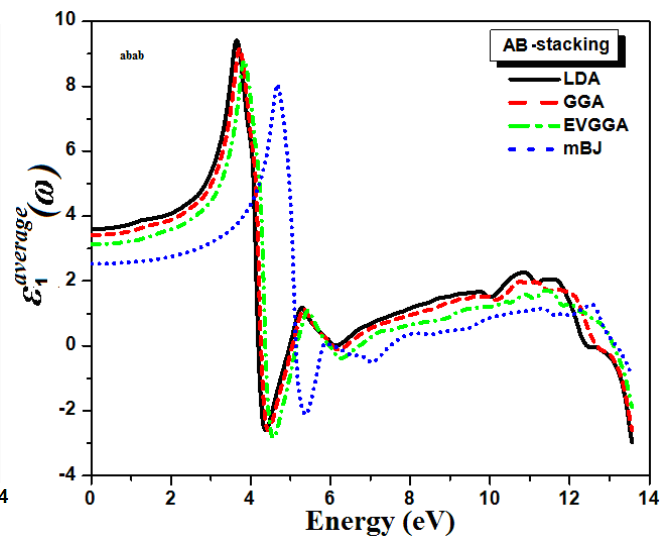


Fig. 1

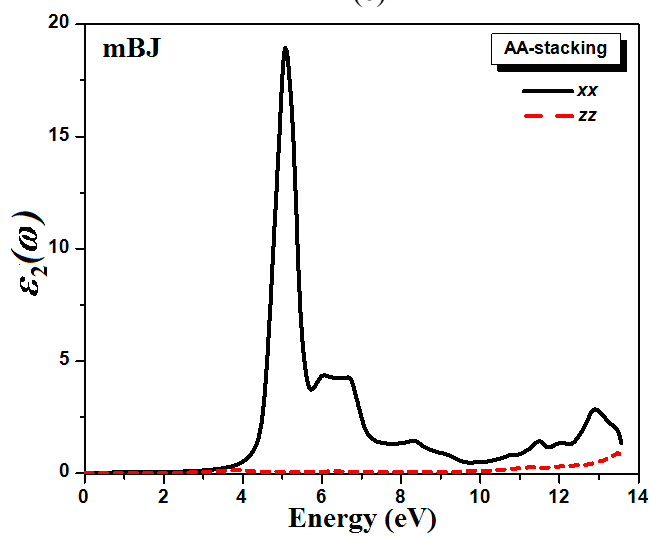




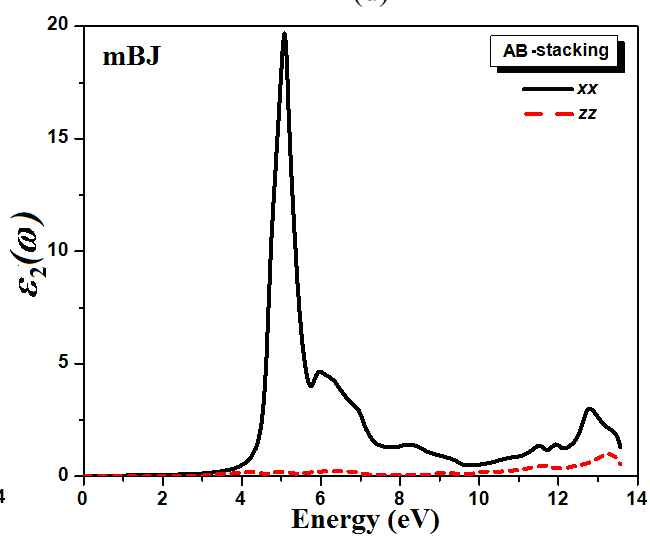
(c)



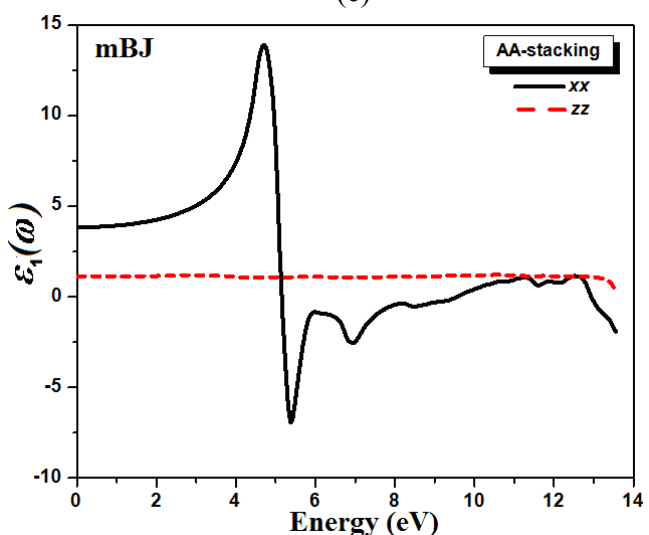
(d)



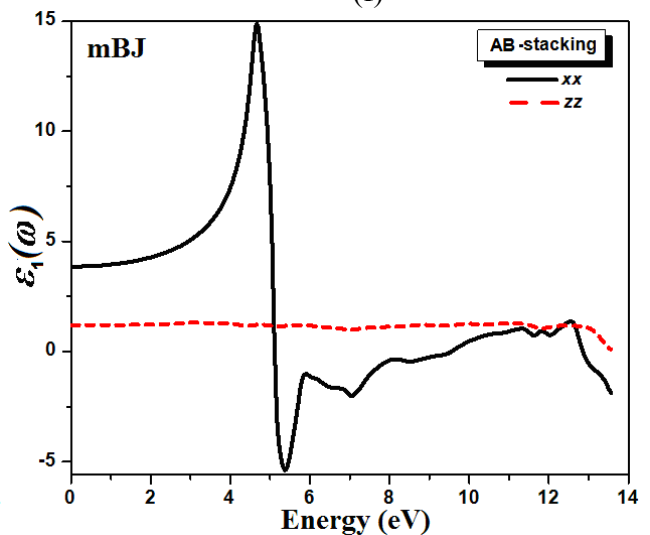
(e)



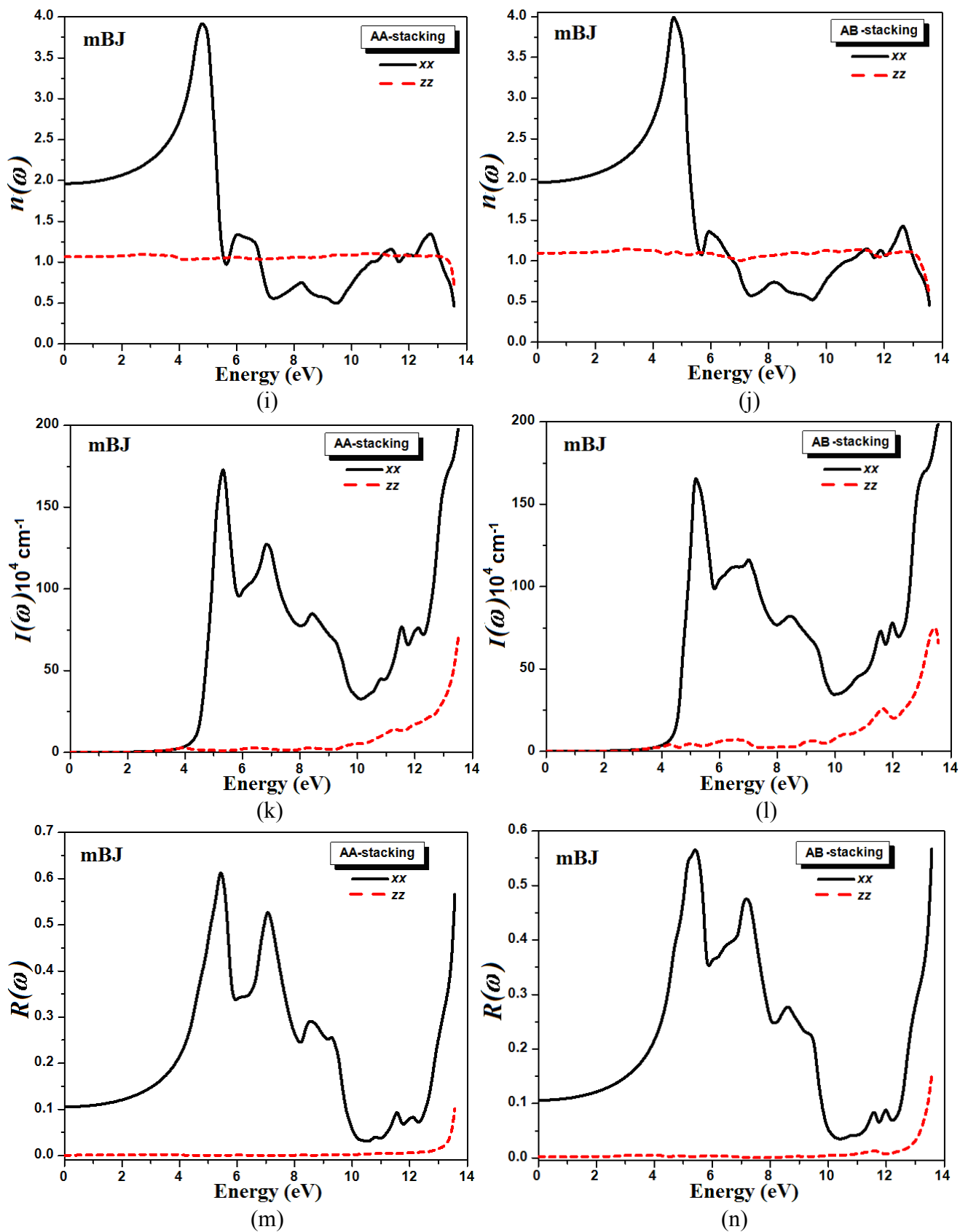
(f)



(g)



(h)



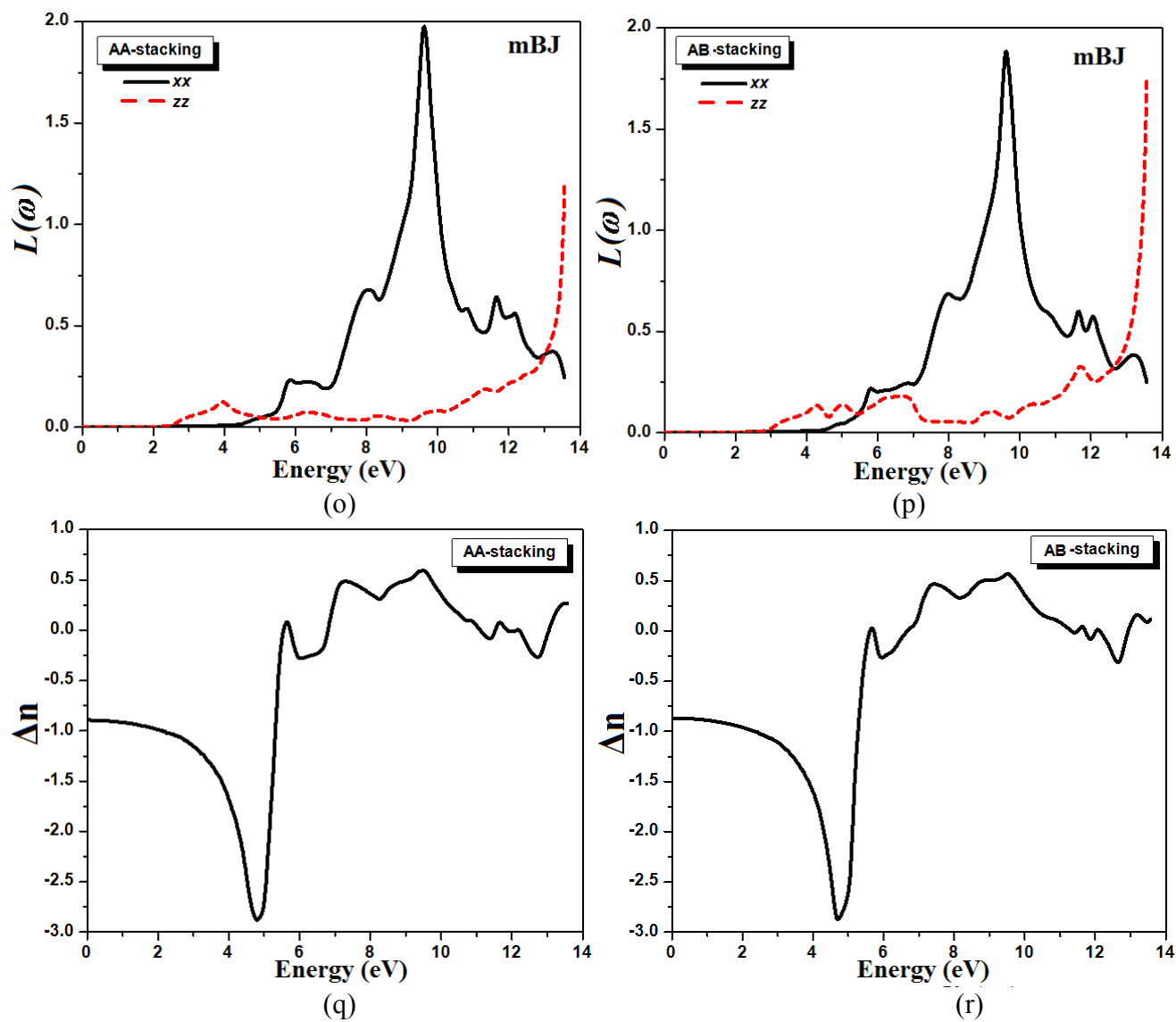
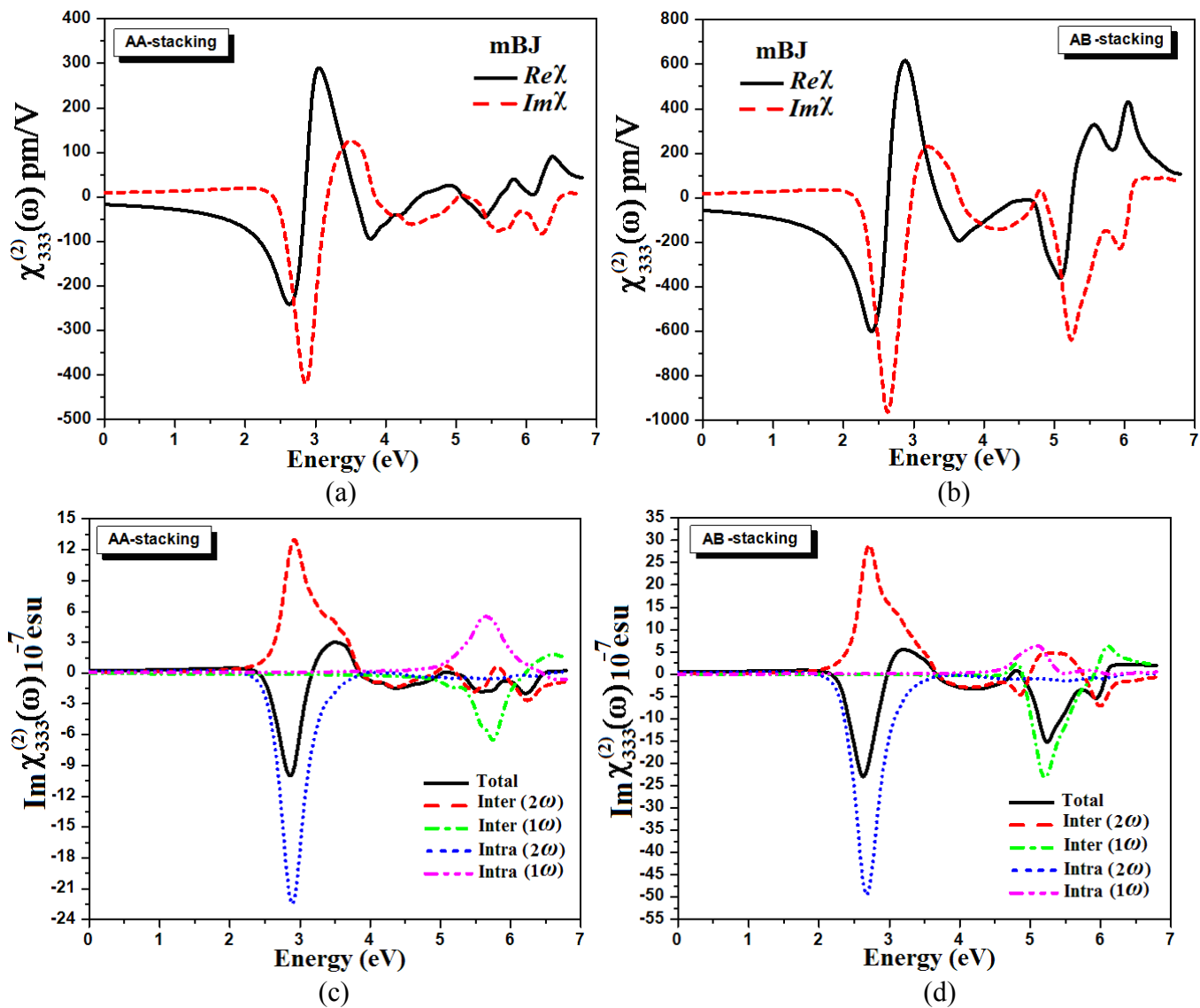


Fig.2



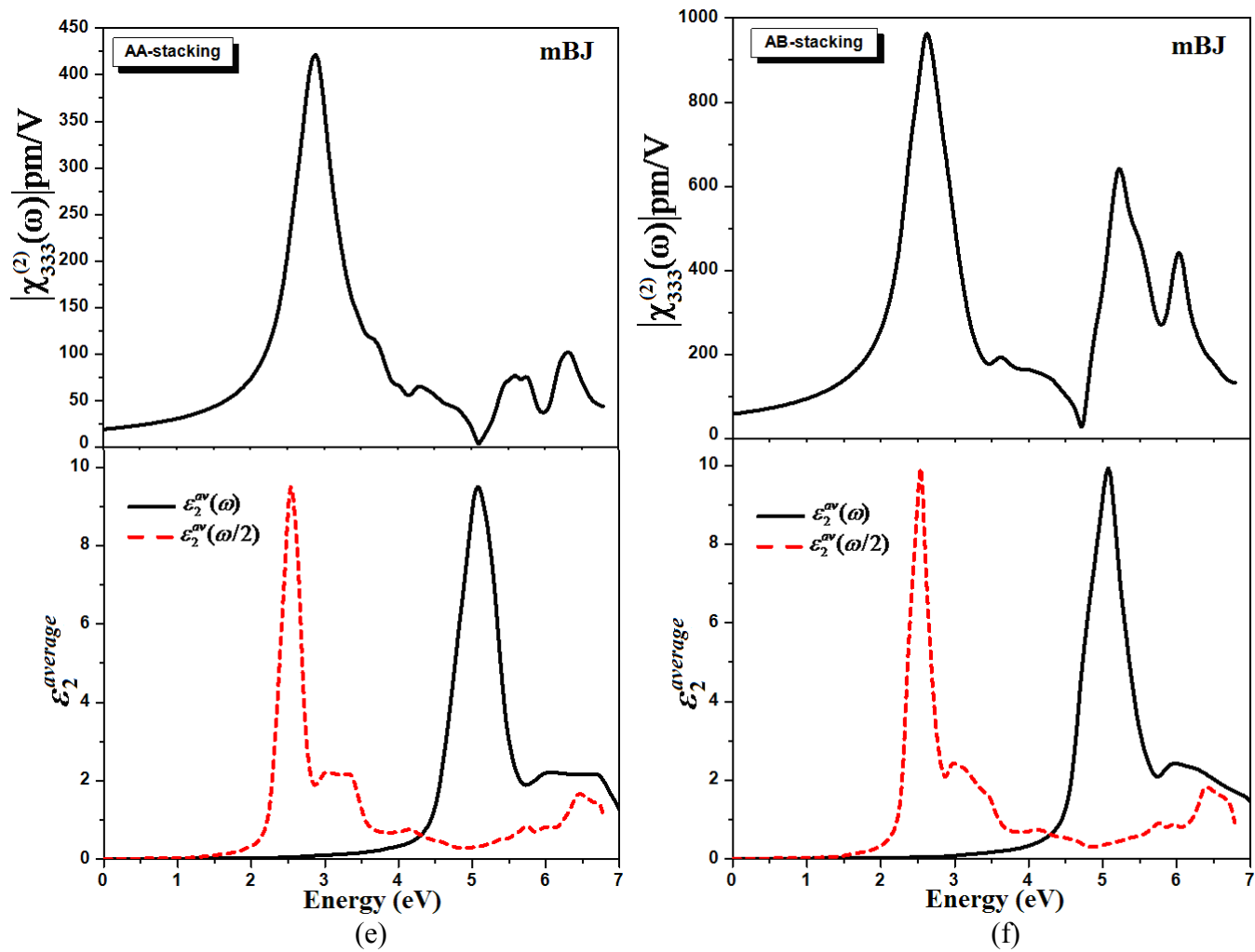


Fig.3